FORECASTING RUNOUT OF ROCK AND DEBRIS AVALANCHES

R.M. IVERSON*
U.S. Geological Survey
1300 SE Cardinal Ct. #100, Vancouver, WA 98683 USA

Abstract

Physically based mathematical models and statistically based empirical equations each may provide useful means of forecasting runout of rock and debris avalanches. This paper compares the foundations, strengths, and limitations of a physically based model and a statistically based forecasting method, both of which were developed to predict runout across three-dimensional topography. The chief advantage of the physically based model results from its ties to physical conservation laws and well-tested axioms of soil and rock mechanics, such as the Coulomb friction rule and effective-stress principle. The output of this model provides detailed information about the dynamics of avalanche runout, at the expense of high demands for accurate input data, numerical computation, and experimental testing. In comparison, the statistical method requires relatively modest computation and no input data except identification of prospective avalanche source areas and a range of postulated avalanche volumes. Like the physically based model, the statistical method yields maps of predicted runout, but it provides no information on runout dynamics. Although the two methods differ significantly in their structure and objectives, insights gained from one method can aid refinement of the other.

1. Introduction

Forecasts of hazards from rock and debris avalanches must address two kinds of questions: (1) where and when will slope failure occur, and (2) how far and how fast will down-valley runout occur? Although runout of rock avalanches is commonly regarded as a enigmatic phenomenon, forecasting runout may be a more tractable problem than forecasting the location and timing of rock slope failure that occurs in the absence of observed precursory deformation. Whereas slope failure is governed by a balance of quasistatic forces that can be exceedingly delicate (*e.g.*, a factor of safety ~ 1.001 implies that a slope is stable but precariously poised), rock avalanche motion is governed by an imbalance of dynamic forces that can be immense. The speeds and masses of moving rock avalanches dictate that bulk inertial effects commonly dominate motion, and the laws of classical mechanics dictate that the effects of bulk inertia are relatively predictable. Thus, there is cause for optimism about forecasting avalanche runouts.

* *E-mail of author*: riverson@usgs.gov

S.G. Evans et al. (eds.), Landslides from Massive Rock Slope Failure, 197–209.

As might be expected for a phenomenon driven by gravity and dominated by inertia, runout of rock avalanches depends strongly on avalanche volume (or mass) and runout-path topography [15]. The topography of prospective avalanche paths is generally well known, whereas the volumes of prospective avalanches are typically poorly constrained because the size of slope failures commonly depends on subtle geological structures and heterogeneities, and on transient forcing due to rainfall or earthquakes. Therefore, methods for forecasting runout should take advantage of reliable knowledge of topography and take account of limited knowledge of avalanche volume. These considerations argue strongly for use of forecasting methods that represent three-dimensional topographic effects rigorously and treat avalanche volumes as independent variables that have inherent uncertainty.

This paper discusses two methods of forecasting rock avalanche runouts across three-dimensional terrain. One method aims mainly at enhancing scientific understanding by devising a physically and mathematically rigorous theory that yields testable predictions of runout dynamics. The other method aims mainly at expediting practical hazard assessment by using statistical analysis of runout trends to forecast the probable extent of future runouts. The physically based model yields greater returns of information, at a cost of greater demands for input data and computation. The statistically based approach has a more limited scope, but it requires relatively modest computation and no input data other than path topography and a postulated distribution of avalanche volumes.

The choice of a particular method of runout forecasting depends principally on the objectives of the forecast. Some practical objectives (*e.g.*, hazard-zone assessment) may be met most expediently with statistically based methods, whereas scientific objectives (*e.g.*, improved understanding) can be met most rigorously with physically based models. Diverse objectives and methodologies can be synergistic, however. Improved physical understanding can lead to improved hazard forecasts, and information gained in hazard assessments can lead to improved physical understanding.

2. Physically Based Modeling

This section describes formulation and testing of a physically based model that uses universal principles (*i.e.*, mass and momentum conservation) and well-tested formulas (*i.e.*, the Coulomb friction rule and Terzaghi effective-stress principle) to compute avalanche motion from initiation to deposition. The model, developed by Iverson and Denlinger [3, 11], predicts the behavior of granular avalanches under a wide variety of soil and rock states, which may range dry to water-saturated and from rigid to fully fluidized. Conditions in which the model applies include static limiting equilibrium (which exists at the onset of slope failure), dynamic states dominated by bulk inertia, and subsequent static states that result from deposition. Furthermore, the model accounts for the effects of evolving pore-fluid pressure and three-dimensional path topography.

2.1. CONCEPTUAL FRAMEWORK

The guiding philosophy of the model of Iverson and Denlinger [3, 11] is to represent the well-constrained aspects of avalanche dynamics as thoroughly as practicably possible, and to minimize assumptions about the more puzzling aspects of avalanche dynamics. For example, aspects of avalanche dynamics dictated by momentum conservation are

completely constrained by physical law. Therefore, bulk inertia terms (which express momentum transport without energy dissipation) in the avalanche dynamics model involve no assumptions, and involve only mathematical approximations that are rigorously justifiable in view of the pertinent physics.

The more puzzling aspects of avalanche dynamics result from dissipative (*i.e.*, resisting) forces, and the model assumes that these forces obey well-tested formulas of classical soil and rock mechanics (*i.e.*, the rules for Coulomb friction and effective stress mediated by pore-fluid pressure). This parsimonious approach to physically based modeling provides the surest route to rigorous understanding of avalanche runout, because it employs no coefficients that are adjusted to fit model predictions to data, and it thereby facilitates conclusive hypothesis tests. Use of adjustable resisting forces in avalanche dynamics models is unwarranted unless a model that rigorously conserves momentum and employs parsimonious assumptions about resisting forces is demonstrably inadequate [10].

2.2. MATHEMATICAL FORMULATION

As noted above, the central postulate in the avalanche dynamics model of Iverson and Denlinger [3, 11] is the well-known Coulomb-Terzaghi equation for resistance to basal sliding:

$$\tau_{bed} = (\sigma_{bed} - p_{bed}) \tan \varphi_{bed} \tag{1}$$

Here σ_{bed} is basal normal stress, p_{bed} is basal pore-fluid pressure, and φ_{bed} is the basal Coulomb friction angle, which is constrained by experiments to range from about 30 to 40 degrees for most fragmented rocks and granular soils. Application of the Coulomb-Terzaghi equation to avalanche dynamics involves a number of subtleties, however. *First*, a resistance equation consistent with Coulomb-Terzaghi behavior must be employed to describe not only basal sliding but also shear and normal stresses within deforming avalanches. *Second*, basal pore-fluid pressure in an avalanche mass can change as a function of position and time, and evolving pore-fluid pressure must therefore be evaluated simultaneously with evolving avalanche motion. *Third*, mass and momentum must be conserved in four dimensions (space plus time) within the moving avalanche.

A detailed mathematical derivation of equations with the properties described above is beyond the scope of this summary but has been provided by Iverson and Denlinger [11]. To simplify the four-dimensional equations, they are integrated through the avalanche thickness to eliminate explicit dependence on the velocity component normal to the bed. This simplification is typically justifiable because tabular avalanche geometries dictate that bed-normal velocities are much smaller than bed-parallel velocities in most instances [18, 19]. The resulting depth-integrated equations governing evolution of mass, momentum and pore-pressure distributions are referenced to a coordinate system fitted to local bed topography (Figure 1) and are summarized as follows:

$$\frac{\partial \mathrm{U}}{\partial t} + \frac{\partial \mathrm{F}}{\partial x} + \frac{\partial \mathrm{G}}{\partial y} = \mathrm{S} \tag{2a}$$

where

$$\mathrm{U} = \begin{bmatrix} h \\ h\,\overline{\nu}_x \\ h\,\overline{\nu}_y \\ \lambda h \end{bmatrix} \quad \mathrm{F} = \begin{bmatrix} h\,\overline{\nu}_x \\ h\,\overline{\nu}_x^2 + \frac{1}{2} h\,c^2 \\ h\,\overline{\nu}_x\,\overline{\nu}_y \\ \lambda h\,\overline{\nu}_x \end{bmatrix} \quad \mathrm{G} = \begin{bmatrix} h\,\overline{\nu}_y \\ h\,\overline{\nu}_y\,\overline{\nu}_x \\ h\,\overline{\nu}_y^2 + \frac{1}{2} h\,c^2 \\ \lambda h\,\overline{\nu}_y \end{bmatrix} \quad \mathrm{S} = \begin{bmatrix} 0 \\ S_x \\ S_y \\ S_\lambda \end{bmatrix} \tag{2b,c,d,e}$$

$$S_x = g_x\,h - \mathrm{sgn}(\overline{\nu}_x)(1-\lambda)\left(g_z + \overline{\nu}_x^2\,\frac{\partial\,\theta_x}{\partial x}\right) h \tan\varphi_{bed} - \frac{3\,\upsilon_f\,\mu}{\rho}\,\frac{\overline{\nu}_x}{h} \tag{2f}$$
$$+\frac{\upsilon_f\,\mu h}{\rho}\,\frac{\partial^2\,\overline{\nu}_x}{\partial\,x^2} - \mathrm{sgn}\left(\frac{\partial\,\overline{\nu}_x}{\partial y}\right) h\,k_{act/pass}\,\frac{\partial}{\partial y}[g_z\,h(1-\lambda)]\sin\varphi_{int} + \frac{\upsilon_f\,\mu h}{\rho}\,\frac{\partial^2\,\overline{\nu}_x}{\partial\,y^2}$$

$$S_y = g_y\,h - \mathrm{sgn}(\overline{\nu}_y)(1-\lambda)\left(g_z + \overline{\nu}_y^2\,\frac{\partial\,\theta_y}{\partial y}\right) h \tan\varphi_{bed} - \frac{3\,\upsilon_f\,\mu}{\rho}\,\frac{\overline{\nu}_y}{h} \tag{2g}$$
$$+\frac{\upsilon_f\,\mu h}{\rho}\,\frac{\partial^2\,\overline{\nu}_y}{\partial\,y^2} - \mathrm{sgn}\left(\frac{\partial\,\overline{\nu}_y}{\partial x}\right) h\,k_{act/pass}\,\frac{\partial}{\partial x}[g_z\,h(1-\lambda)]\sin\varphi_{int} + \frac{\upsilon_f\,\mu h}{\rho}\,\frac{\partial^2\,\overline{\nu}_y}{\partial\,x^2}$$

$$S_\lambda = \frac{D}{\rho\,g_z\,h}\,\frac{2}{\lambda_0}\left(\frac{\partial p}{\partial z}\,|_h + \rho_f g_z\right) \tag{2h}$$

$$k_{act/pass} = 2\frac{1 \mp [1 - \cos^2\varphi_{int}(1 + \tan^2\varphi_{bed})\,]^{1/2}}{\cos^2\,\varphi_{int}} - 1 \tag{2i}$$

$$\lambda = \frac{p_{bed}}{\rho\,g_z\,h} \qquad c = \sqrt{[(1-\lambda)\,k_{act/pass} + \lambda]\,g_z\,h} \tag{2j,k}$$

Although this set of equations is mathematically complex, the physical concepts entailed are simple and few: mass and momentum conservation, Coulomb friction, and effective stress mediated by evolving pore-fluid pressure. The independent variables in the equations are the orthogonal planimetric coordinates *x* and *y* (which are rotated to fit local

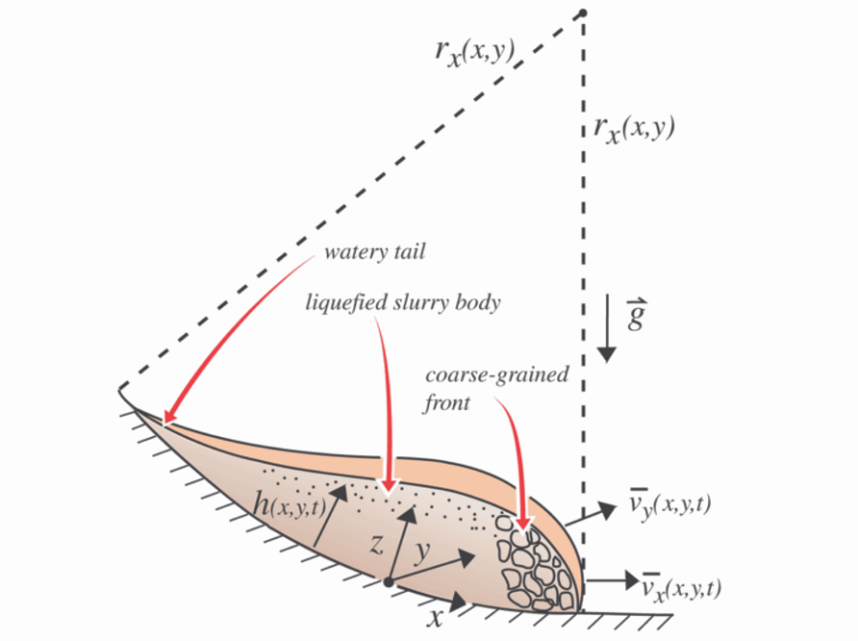

Figure 1. Schematic illustrating variables in the avalanche model summarized by equations (2 a-k). Vertical exaggeration is about 10 to 100×. Labels of the front, body, and tail characterize an avalanche or debris flow that is partially liquefied by high pore-water pressure.

topography) and time t. The dependent variables are the depth-integrated velocity components $\bar{v}_x(x, y, t)$ and $\bar{v}_y(x, y, t)$, the avalanche thickness $h(x, y, t)$, and the basal pore-pressure ratio, $\lambda(x, y, t)$. For granular avalanches without pore-fluid effects (*i.e.*, $\mu = 0, \lambda = 0$), the only relevant parameters are the basal and internal friction angles of the granular debris, ϕ_{bed} and ϕ_{int}. If pore-fluid effects are present, additional relevant parameters are the bulk density of the avalanche debris, ρ, bulk density of the pore fluid, ρ_f, volume fraction of the pore fluid (*i.e.*, porosity), υ_f, viscosity of the pore fluid, μ, and the pore-pressure diffusivity (*i.e.*, consolidation coefficient), D. The x and y components of gravitational acceleration, g, local slope angle, θ, and local bed curvature, $1/r_x = \partial\theta_x/\partial x$, are determined by the local terrain (Figure 1). An important feature of all of these quantities is that they are independently measurable on maps or in standard laboratory tests; none of the quantities is an adjustable tuning coefficient.

The equations defining $k_{act/pass}$, λ, and c are mathematically derived and have straightforward physical interpretations [3, 9, 11]: $k_{act/pass}$ is a Rankine earth-pressure coefficient that applies in cases with simultaneous internal deformation and slip along the bed; λ is the ratio of basal pore pressure to basal lithostatic stress; and c is a gravity-wave speed that governs the maximum rate at which disturbances propagate longitudinally

through the deforming avalanche material. In general this gravity-wave speed is influenced by intergranular friction and includes as a special case the analogous speed used in shallow-water wave theory, $c = (g_z h)^{1/2}$. Here, $c = (g_z h)^{1/2}$ applies only under conditions of full avalanche fluidization ($\lambda = 1$).

Initial conditions used to begin model calculations specify zero avalanche velocity ($\bar{v}_x = \bar{v}_y = 0$), an initial pore-pressure distribution, $\lambda_0(x, y)$, and an initial thickness distribution $h_0(x, y)$. The thickness distribution defines the avalanche volume, which is assumed to remain constant throughout motion and deposition. Terms that allow for variable avalanche volume due to progressive erosion or sedimentation can easily be added to the mass- and momentum-conservation equations. To date, however, no rigorous experiments or calculations have been performed to constrain the magnitude of such terms, and they consequently are omitted. To assess behavior of prospective avalanches with differing initial volumes or distributions of mass as specified by $h_0(x, y)$, multiple model runs are required.

The system of equations (2a-k) listed above includes some well-known equations as special cases: the standard shallow-water equations [22], the dry granular avalanche equations of Savage and Hutter [18, 19], the multidimensional Savage-Hutter equations of Gray *et al.* [4], the simplified Savage-Hutter equations of Hungr [7], and the sliding-consolidation equations of Hutchinson [8]. Also, despite their generality, equations (2a-k) contain at their core the simple one-dimensional equation of motion for a rigid Coulomb slide block,

$$d\bar{v}_x/dt = g(\sin\theta - \cos\theta \tan\varphi_{bed}) \tag{3}$$

The mathematical complexity that distinguishes (2a-k) from (3) is necessary to account for the distributions of velocity, thickness and pore pressure in three-dimensional rock and debris avalanches.

2.3. MODEL TESTING

One of the biggest obstacles to developing a robust, physically based model of rock and debris avalanches is the difficulty of conclusive testing. Such models can seldom, if ever, be tested against field data, because field data generally leave many factors (such as initial and boundary conditions) poorly constrained. Therefore, models are generally *fitted to* field data rather than *tested against* field data, and model veracity remains equivocal.

As an alternative to fitting field data, models can be tested against data from controlled experiments in which all parameter values, boundary conditions, and initial conditions are independently constrained. However, a potential difficulty with such experiments is *scaling*, because controlled experiments generally cannot be conducted at the scale of large geological events. This difficulty can be addressed in several ways. For example, normalization of the equations of motion (2a-k) identifies relevant scaling parameters, which imply that purely frictional avalanches without pore-fluid effects will behave in a manner that is independent of scale [11]. On the other hand, the same scaling parameters indicate that avalanches with pore-fluid effects can be expected to behave in a scale-dependent manner, whereby increasing mobility occurs with increasing scale if all other

factors are constant. These scaling considerations motivated Denlinger and Iverson [3] to test model predictions against data from two kinds of experiments: (1) bench-top experiments with miniature avalanches of about 0.001 m^3 of dry, well-sorted sand in which pore-fluid effects were negligible, and (2) large-scale, outdoor experiments with avalanches of about 10 m^3 of poorly sorted, water-saturated sand and gravel with significant pore-fluid effects. Both types of experiment highlighted the importance of multidimensional momentum transport in avalanches, and both demonstrated good agreement between data and model predictions. However, owing to the complexity of the numerical method used to compute solutions to the model equations, additional testing under more realistic scenarios with complex topography and boundary conditions is necessary before runout predictions of natural rock avalanches can be made with confidence.

Experiments like those reported by Denlinger and Iverson [3] also reveal phenomena that provoke new kinds of questions and motivate further model refinements. For example, experiments show that grain-size segregation can be an extremely efficient process in poorly sorted avalanches. This segregation influences pore-pressure generation and dissipation (because fine sediments sustain high pore pressures more readily than do coarse aggregates,) and it therefore holds large implications for macroscopic dynamics. Indeed, feedbacks between the micro-dynamics of grain-scale processes and the macro-dynamics of avalanche motion may be crucial in some circumstances [13]. Such complexities demonstrate the need for continuing efforts to refine physically based models.

3. Statistically Based Forecasting

The complexity of rigorous, physically based modeling of rock avalanche runout indicates a need for simpler forecasting methods that can be readily employed in hazard assessments. Commonly such assessments must be performed in situations where limitations of time, money, or information preclude detailed modeling. The summary below describes a statistical forecasting method developed by Iverson *et al.* [12] to delineate areas likely to be inundated by lahars, which are water-saturated debris flows that originate on volcanoes. With modification of the pertinent data sets and statistics, as summarized below, this method can be adapted to forecasting runout of rock and debris avalanches.

3.1. CONCEPTUAL FRAMEWORK

The framework of this forecasting method rests on three observations: (1) the primary factor determining runout of a prospective rock avalanche is its volume, but this volume is unknown *a priori*; (2) a secondary factor determining runout is the three-dimensional topography of potential runout paths, which may be known with good accuracy as a result of standard topographic mapping; (3) runout patterns of large avalanches appear geometrically similar to those of small avalanches viewed at a larger scale. That is, runout patterns appear to exhibit fractal scaling.

In accord with these observations, the forecasting methodology described here entails formulation and statistical testing of empirical, scale-independent runout equations that employ avalanche volume as the independent variable. In this methodology a range of avalanche volumes is postulated and used to compute runout zones that are constrained by

path topography. The computed runout zones reflect both the statistical uncertainty of the runout equations and geological uncertainty about prospective avalanche volumes.

The possibility of valid, scale-independent runout equations has been suggested previously. Many investigators have noted that runout of rock avalanches is characterized better by the planimetric area inundated than by Heim's [5] famous fahrböschung or H/L ratio [1, 2, 6, 12, 14, 15, 16, 21]. Whereas H/L ratios decline markedly and nonlinearly with increasing avalanche volume (V), planimetric areas of inundation (A_1) scale quite consistently with $V^{2/3}$, as might be expected on the basis of the dimensional equivalence of A_1 and $V^{2/3}$. Thus, the power-law hypothesis

$$A_1 = \alpha_1 V^{2/3} \tag{4}$$

where α_1 is a constant, can be assessed statistically to evaluate whether it provides a useful runout equation that is independent of scale.

$$A_2 = \alpha_2 V^{2/3} \tag{5}$$

Although equation (4) may be useful for assessing runout, by itself it is insufficient for delineating runout zones, because it provides no information about the spatial distribution of A_1. An additional equation is needed to constrain the lateral limits of inundation and thereby place planimetric bounds on the area defined by A_1. On the basis of physical scaling arguments detailed by Iverson *et al.* [12], an additional power-law equation is postulated to relate the maximum vertical cross-sectional area of valley inundation (A_2) to the avalanche volume. This equation constrains the lateral limits of inundation if the runout path topography is known. If initiation areas and avalanche volumes are specified, use of equation (5) in conjunction with equation (4) defines the extent of prospective avalanche runout zones. Of course, the utility of this approach depends on the statistical validity of the hypotheses represented by equations (4) and (5).

3.2. STATISTICAL BASIS

A complete description of the statistical rationale and methods used to test and calibrate runout equations (4) and (5) was provided by Iverson *et al.* [12], who applied these equations to lahar runouts. For the rock avalanche runouts addressed here, a detailed report is in preparation; the results summarized below aim only to demonstrate the potential viability of the method.

As an initial step in statistical testing and calibration, equations (4) and (5) are logarithmically transformed to the linear forms,

$$\log A_1 = \log \alpha_1 + \tfrac{2}{3} \log V \tag{6a}$$

$$\log A_2 = \log \alpha_2 + \tfrac{2}{3} \log V \qquad (6b)$$

The log transformation facilitates use of least-squares linear regression as a tool for testing and calibration, and also implies that scatter of observed values of A_1 and A_2 as functions of V is expected to scale with the magnitude V.

Table 1 summarizes results of statistical testing and calibration of (6a) and (6b) using published data for rock avalanches worldwide. Published data on planimetric innundation area A_1 are common, whereas published data on valley cross-sectional inundation area A_2 are rare. Therefore, different sets of avalanches were used to compile the data for testing (6a) and (6b), and using these disparate data sets it is not feasible to assess the possibility of cross-correlation between the A_1 and A_2 values. Instead, the data sets for A_1 and A_2 are treated as completely independent.

The most important information in Table 1 is provided by the F statistics, which compare alternative linear models of log A_1 and log A_2 as functions of log V. Very large values of the F statistic for the "specified zero slope" models indicate that such models can be rejected with a high degree of confidence (exceeding 99.5 %, as inferred from tabulated values of the F distribution). In other words, regression models that assume linear dependencies of log A_1 and log A_2 on log V are clearly superior to models that assume log A_2 and log A_1 lack dependence on log V. In contrast, the small values of the F statistic for the "specified 2/3 slope" models indicate that such models cannot be rejected with even a 90% degree of confidence. In other words, the 2/3 power laws represented by equations (6a) and (6b) are not clearly distinguishable from the best-fit linear regressions representing log A_1 and log A_2 as functions of log V. On this basis the 2/3 power laws are adopted as acceptable models of the data.

Calibration of the 2/3 power laws entails determining optimal values of the coefficients α_1 and α_2. To accomplish this, best-fit values of α_1 and α_2 are obtained by minimizing the mean square error in (6a) and (6b) (as in a linear regression procedure), and then rounding these values to two significant digits. In this way $\alpha_1 = \log^{-1}(1.3617) = 23$ and $\alpha_2 = \log^{-1}(\text{-}0.699) = 0.20$ are obtained, yielding the predictive equations

$$A_1 = 23\, V^{2/3} \qquad A_2 = 0.20\, V^{2/3} \qquad (7a,b)$$

The forms of these equations are similar to those of equations used by Iverson *et al.* [12] to forecast lahar inundation, but the coefficients that multiply $V^{2/3}$ are unique to rock avalanches. For rock avalanches, the planimetric runout coefficient 23 replaces the lahar coefficient 200, and the cross-sectional inundation coefficient 0.20 replaces the lahar coefficient 0.05. Thus, on the basis of these coefficients, rock avalanches can be expected to inundate planimetrtic areas about nine times smaller than those inundated by lahars of similar volume and can be expected to inundate valley cross-sectional areas about four times larger than those inundated by lahars of similar volume. These contrasts reflect the fact that rock avalanches generally undergo less liquefaction and exhibit more flow resistance than lahars.

Table 1. Parameters and analysis-of-variance statistics for alternative linear models of log-transformed runout data for rock avalanches.

	Models for prediction of planimetric inundation area, A_1		
Parameter	Best-fit regression	Specified 2/3 slope	Specified zero slope
slope of line	0.7207	0.6667	0.0000
intercept of line at log V =0	0.9296	1.3617	6.8146
number of data pairs	136	136	136
degrees of freedom	134	135	135
sum of squares	30.5634	31.1179	127.4689
mean square	0.2281	0.2305	0.9442
standard error	0.4776	0.4801	0.9717
r^2 statistic	0.7602	0.7559	0.0000
F statistic	not applicable	2.4311	424.87
	Models for prediction of cross-sectional inundation area, A_2		
Parameter	Best-fit regression	Specified 2/3 slope	Specified zero slope
slope of line	0.6304	0.6667	0.0000
intercept of line at log V =0	-0.3971	-0.699	4.7077
number of data pairs	12	12	12
degrees of freedom	10	11	11
sum of squares	1.9930	2.0182	9.3434
mean sqaure	0.1993	0.1835	0.8494
standard error	0.4464	0.4283	0.9216
r^2 statistic	0.7867	0.7840	0.0000
F statistic	not applicable	0.1262	36.88

The uncertainty of the runout forecasts obtained from equations (7a) and (7b) can be estimated from the associated standard errors, which fall between 0.4 and 0.5 (Table 1). Because these values apply to log-transformed data, they imply standard errors of about $10^{0.4}$ to $10^{0.5}$ ($\approx$ 3) for constraining either A_1 or A_2 as a function of V. At first glance the three-fold standard error associated with (7a) and (7b) might seem unacceptably large for runout forecasting, but the error appears less severe if uncertainty associated with postulating prospective avalanche volumes V is considered concurrently. In most hazard assessments, only broad bounds can be placed on V, and a population of possible avalanche volumes must be postulated to provide a useful forecast. Thus, the standard error associated with using (7a) and (7b) to forecast inundation by an avalanche with a particular V must be gaged relative to the uncertainty about V itself. Viewed in this context, a threefold standard error associated with (7a) and (7b) appears tolerable. Of course, any hazard assessment that employs (7a) and (7b) superposes the uncertainty of the equations and the uncertainty in postulated ranges of V to produce a runout forecast that is probabilistic, not deterministic.

3.3. EXAMPLE OF APPLICATION

The implications of the uncertainties associated with (7a) and (7b) are illustrated by example in Figure 2, which depicts a map that forecasts rock avalanche runout patterns on

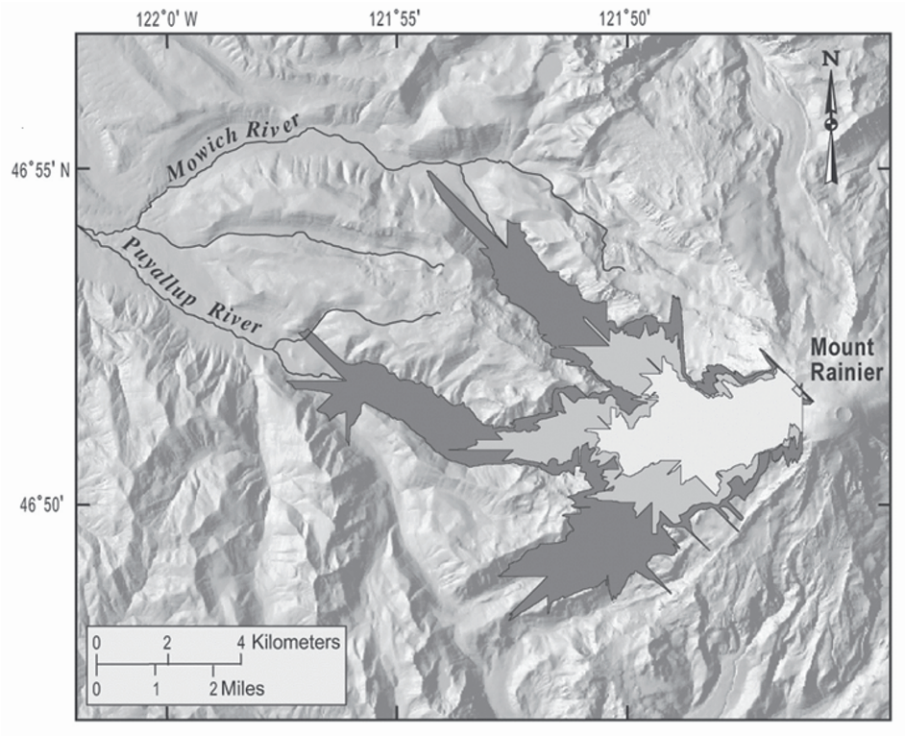

Figure 2. Shaded relief map of the western flank of Mt. Rainier, Washington, USA, with runout hazard zones for rock avalanches originating in the Sunset Amphitheater. Nested hazard zones were computed for avalanches with hypothetical volumes of 0.1 km^3 (light tone), 0.316 km^3 (intermediate tone), and 1 km^3 (dark tone) that might descend one or more of three valleys.

the western flank of Mount Rainier, Washington, USA. The algorithm used to compute these avalanche inundation patterns is the same as that described by Iverson et al. [12] and Schilling [20] for computing lahar inundation patterns; only the coefficients in (7a) and (7b) are novel. The spiny appearance of the hazard zones depicted in Figure 2 is a consequence of the relatively coarse resolution (62.5 m) of the digital elevation model (DEM) used to represent Mount Rainier's topography. Spines tend to disappear if DEMs with finer resolution are employed (S.P. Schilling, personal communication, 2002).

To generate the hazard zones depicted in Figure 2, a prospective avalanche source area in and around the steeply sloping Sunset Amphitheater at about 4000 m elevation on the western flank of Mount Rainier was chosen. On the basis of its geometry, lithology, and geological history, the Sunset Amphitheater has been identified as an area particularly susceptible to slope failure [17]. To compute the three nested hazard zones in Figure 2, three values of V were postulated: 0.1 km^3, 0.316 km^3, and 1 km^3, corresponding to log V = -1, -0.5, and 0, respectively. This ten-fold range in V results in a 4.64-fold variation in the predicted inundation areas A_1 and A_2 (because $10^{2/3} \approx 4.64$). This variation is about 50%

larger than the three-fold variation of inundation areas expected on the basis of the standard errors of equations (7a) and (7b). Thus, the inner hazard zone in Figure 2 would almost certainly be inundated by an avalanche with $V \sim 0.3$ km^3, and an avalanche of this volume would be very unlikely to inundate an area larger than that of the outer hazard zone in Figure 2. A similar rationale can be extended to smaller and larger avalanches by computing additional inundation areas (for additional postulated V) and depicting them on a map like Figure 2. Iverson *et al.* [12] provide a more thorough discussion and detailed example of this methodology, albeit in the context of lahars rather than rock avalanches.

The hazard zones of Figure 2 illustrate both advantages and limitations of the statistical forecasting method. Depiction of nested hazard zones with specified ranges of uncertainty is a clear advantage in hazard assessments. On the other hand, the depicted hazard zones take no account of dynamic effects (such as runup and superelevation) that occur as avalanches interact with topography, and they provide no information on avalanche speeds and impact forces.

4. Conclusion

Forecasting runout of rock and debris avalanches is a longstanding problem with both scientific and practical importance. Scientific questions about the mechanics of the runout process can be best addressed with a physically based runout model that rigorously conserves momentum and avoids used of adjustable coefficients. On the other hand, practical questions about the likelihood of down-valley inundation can be addressed most expediently with a statistical model developed specifically for hazard assessment. The two methods can be synergistic, however. Elementary physical reasoning leads to scaling relationships that provide some constraints on statistical forecasting by guiding formulation of pertinent empirical equations, and statistically verified empiricisms summarize data trends that can be targets for prediction by rigorous, physically based models. Continued progress in scientific understanding and hazard assessment will likely entail melding of information obtained from physically based and statistically based investigations.

Acknowledgments

Julia Griswold compiled the data and performed the calculations for application of the statistical forecasting method to rock avalanche runout, and she computed the hazard map for the western flank of Mount Rainier (Figure 2) . Steve Schilling wrote the GIS program LAHARZ, which performs the computations.

References

1. Dade, W.B., and Huppert, H.E. (1998) Long-runout rockfalls, *Geology* **26**, 803-806.
2. Davies, T.R.H. (1982) Spreading of rock avalanche debris by mechanical fluidization, *Rock Mech.* **15**, 9-24.
3. Denlinger, R.P., and Iverson, R.M. (2001) Flow of variably fluidized granular masses across three-dimensional terrain: 2. Numerical predictions and experimental tests, *J. Geophys. Res.* **106 B**, 553-566.

4. Gray, J.M.N.T.,Wieland, M., and Hutter, K. (1999) Gravity driven free surface flow of granular avalanches over complex basal topography, *Proc. Roy. Soc. London, Ser. A.* **455**, 1841-1874.
5. Heim, A. (1932) *Bergsturz und Menschenleben*, Fretz and Wasmuth, Zürich.
6. Hungr, O. (1990) Mobility of rock avalanches, *Report of the National Research Center for Disaster Prevention* (Japan) **46**, 11-19.
7. Hungr, O. (1995) A model for the runout analysis of rapid flow slides, debris flows, and avalanches, *Can. Geotech. J.* 32, 610-623.
8. Hutchinson, J.N. (1986) A sliding-consolidation model for flow slides, *Can. Geotech. J.* **23**, 115-126.
9. Iverson, R.M. (1997) The physics of debris flows, *Rev. Geophys.* **35**, 245-296.
10. Iverson, R.M. (2003) How should mathematical models of geomorphic processes be judged? in P.R. Wilcock and R.M. Iverson (eds.) *Prediction in Geomorphology*, Geophys. Monograph 135, American Geophysical Union, Washington, D.C.
11. Iverson, R.M., and Denlinger, R.P. (2001) Flow of variably fluidized granular masses across three-dimensional terrain: 1. Coulomb mixture theory, *J. Geophys. Res.* **106 B**, 537-552.
12. Iverson, R.M. Schilling, S.P., and Vallance, J.W. (1998) Objective delineation of lahar-inundation hazard zones, *Geol. Soc. Amer. Bull.* **110**, 972-984.
13. Iverson, R.M., and Vallance, J.W. (2001) New views of granular mass flows, *Geology* **29**, 115-118.
14. Kilburn, C.R.J., and Sørensen, S-A. (1998) Runout lengths of struzstroms: the control of initial conditions and of fragment dynamics, *J. Geophys. Res.* **103 B**, 17877-17884.
15. Legros, F. (2002) The mobility of long-runout landslides, *Eng. Geol.* **63**, 301-331.
16. Li Tianchi (1983) A mathematical model for predicting the extent of a major rockfall, *Ziets. Geomorph.* 27, 473-482.
17. Reid, M.E., Sisson, T.W., and Brien, D.L. (2001) Volcano collapse promoted by hydrothermal alteration and edifice shape, Mount Rainier, Washington, *Geology* 29, 779-782.
18. Savage, S.B., and Hutter, K. (1989) The motion of a finite mass of granular material down a rough incline, *J. Fluid Mech.* **199**, 177-215.
19. Savage, S.B., and Hutter, K. (1991) The dynamics of avalanches of granular materials from initiation to runout, Part I. analysis, *Acta Mechanica* **86**, 201-223.
20. Schilling, S.P. (1998) LAHARZ: GIS programs for automated delineation of lahar hazard zones, *U.S. Geol. Sur. Open-file Rep. 98-638*.
21. Vallance, J.W., and Scott, K.M. (1997) The Osceola mudflow from Mount Rainier: sedimentology and hazards implications of a huge clay-rich debris flow, *Geol. Soc. Amer. Bull.* **109**, 143-163.
22. Vreugdenhil, C.B. (1994) *Numerical Methods for Shallow-Water Flow*, Kluwer, Dordrecht.